

An effective model for carbon nanotubes

Hsiu-Hau Lin

Department of Physics, University of California, Santa Barbara, CA 93106

(December 2, 2024)

Single-wall carbon nanotubes with on-site interaction $U \ll t$ are studied by a controlled renormalization group method. When formulated as a system of N_f flavors of interacting Dirac fermions, the effective model at generic filling resembles a set of quasi-1D Hubbard chains. For the undoped (N_y, N_y) -armchair and the $(N_x, -N_x)$ -zigzag with $N_x = 3n$, specific mappings to the 2-chain Hubbard model at *half filling* with effective interaction $u_{\text{eff}} = U/N_y$ and $2U/N_x$ are found from this more general equivalence. The phase diagrams of the $(3, 3)$ -armchair and the $(6, -6)$ -zigzag at generic fillings are studied and compared as an example.

I. INTRODUCTION

Carbon nanotubes consist of single or multiple seamless shells of graphite sheets with a diameter of about several nanometers and length up to micron scale. [1] The nanotubes reveal rich varieties of transport properties as metals, semi-metals and semiconductors depending on their radius and helicity. [2–4] Their marvelous mechanical and electrical properties have attracted lots of attention in both theory and experiment since their discovery in 1991. [5] Recent measurements show that crystalline ropes of single-wall nanotubes (SWNT) exhibit metallic transport properties. [6–8] An individual SWNT has been successfully attached to leads in a two-terminal measurement and has indicated clear signatures of a 1D quantum wire. [9] The quasi-1D nature of these nanotubes necessitates the study of interaction effect, which has pronounced influences in low dimensions. A lot of theoretical work focuses on the band structure calculations. [2–4,10,11] The (N, N) -armchair tube with an on-site interaction U has been mapped to the 2-chain Hubbard model with a reduced interaction strength $u_{\text{eff}} = U/N$ at or near half filling by L. Balents and M. P. A. Fisher. [12] Similar approaches with more general interactions are studied independently by Y. Krotov, D. H. Lee, and S. Louie [13]. The correlation effect at generic filling has been addressed so far. In this paper, we study a SWNT at generic filling with an on-site interaction, which turns out similar to the Hubbard chains.

A SWNT is made by rolling up a 2D graphite sheet along the direction of a superlattice vector (N, M) and then identifying all sites related by this vector (for example, see Fig. 1). In this paper, we focus on two specific types of SWNT's, the (N, N) -armchair and the $(N, -N)$ -zigzag. There are equivalent wrappings due to the symmetry of a honeycomb lattice, for example, $(N, 0)$ and $(0, N)$ superlattice vectors also produce zigzag tubes. In the weak coupling limit $U \ll t, t_{\perp}$, it is natural to diagonalize the hoppings and obtain the band structure first. The chemical potential cuts through the bands at N_f pairs of Fermi points, which enable us to formulate the low-energy theory as N_f flavors of interacting Dirac fermions. The Fermi velocities of these fermions can be computed directly from the band structure. Find-

ing all four-fermion vertices generated by the on-site interaction proves to be trickier. Because of the on-site character, the resulting vertices are independent of the underlying lattice structure and are shown similar to the Hubbard chains. To be precise, interactions of a (N_y, N_y) -armchair tube at the filling, where N_f pairs of Fermi points are present, is shown equivalent to the $2N_y$ -chain Hubbard model (with periodic boundary condition) in the N_f partially filled band region. Similarly, interactions of a $(N_x, -N_x)$ -zigzag tube are the same as in the N_x -chain Hubbard model except for the absence of the umklapp interactions in the k_y direction (see below). Knowing the Fermi velocities and initial couplings of interactions, the phase diagram is determined through the renormalization group approach developed previously in Ref. [14,15].

Since the most interesting (feasible) filling is at or near half filling, specific mappings for nanotubes to two-chain systems based on this more general equivalence are studied. We found that the *undoped* (N_y, N_y) -armchair and the $(N_x, -N_x)$ -zigzag with $N_x = 3n$ are equivalent to the two-chain Hubbard model at *half filling* with effective interaction $u_{\text{eff}} = U/N_y$ and $2U/N_x$ respectively. Unlike the previously mentioned $2N_y$ - and N_x -chain Hubbard model mappings, which only consider interactions, the mappings to the two-chain models takes into account interactions as well as Fermi velocities (band structure). In fact, detailed calculations show that couplings of the N -chain Hubbard with an on-site interaction U in the $N_f = 2$ region are *identically* the same as the 2-chain model with reduced coupling strength $2U/N$ (see below). The possibility of finding the mappings to the 2-chain model relies crucially on the fact that the armchair and the zigzag ($N_x = 3n$) have the same Fermi velocities (band structure) as the real 2-chain model at half filling.

The phase diagrams of the $(3,3)$ -armchair and the $(6, -6)$ -zigzag both of which resemble a 6-chain system, are analyzed by the RG approach. At half filling, both of them acquire charge and spin gaps caused by interactions and thus are expected to be Mott's insulators at zero temperature instead of metals predicted by simple band calculation. Upon slight doping into the $N_f = 2$ region, both become superconductors (SC's) as in the doped 2-chain Hubbard model. The numerical results of the RG

analysis indicate that the armchair has a higher critical temperature than the zigzag. Larger doping makes the armchair (zigzag) enter $N_f=6$ (4) regime where superconductivity is destroyed.

The paper is organized as following. In Sec II, nanotubes at or near half filling, i.e. $N_f = 2$, are studied and mapped to equivalent 2-chain models. In Sec III, nanotubes at generic fillings are considered. By formulating into N_f flavors of interacting Dirac fermions, the equivalence of couplings for nanotubes and the Hubbard ladders is established. In the last section, implications of RG analysis and other theoretical approaches are discussed. Long-range interaction effects and open questions are also discussed, followed by a brief summary of the main conclusions.

II. NANOTUBES AT OR NEAR HALF FILLING

Following many authors [2–4], we consider a 2D graphite sheet first and then take account of finite radius and curvature effects of real tubes. A single sheet of graphite is composed of carbon atoms on the sites of a honeycomb lattice which is a triangle Bravais lattice with two carbon atoms separated by distance d in each unit cell as shown in Fig. 1. The sp_2 electrons of each atom form three bonds with their neighbors and the remaining single p_z electron can tunnel around. Since the honeycomb lattice is bipartite, the nearest neighbor hoppings can be viewed as tunneling alternatively between two triangle sublattices. A tight-binding model at half filling (one electron per site) is introduced to describe electron hoppings in a graphite sheet

$$H_0 = \sum_{\mathbf{r} \in \mathbf{R}, \alpha} \left\{ -tc_{1\alpha}^\dagger(\mathbf{r})c_{2\alpha}(\mathbf{r} + \mathbf{a}_+ + \mathbf{d}) -tc_{1\alpha}^\dagger(\mathbf{r})c_{2\alpha}(\mathbf{r} + \mathbf{a}_- + \mathbf{d}) -t_\perp c_{1\alpha}^\dagger(\mathbf{r})c_{2\alpha}(\mathbf{r} + \mathbf{d}) + \text{h.c.} \right\}, \quad (2.1)$$

where $\mathbf{R} = n_+\mathbf{a}_+ + n_-\mathbf{a}_-$ is the lattice vector of a triangle lattice with bases $\mathbf{a}_\pm = a(\pm 1/2, \sqrt{3}/2)$. The displacement vector between these two triangle sublattices is $\mathbf{d} = a(0, -1/\sqrt{3})$ and $c_i(c_i^\dagger)$ is the fermion annihilation (creation) operator on the corresponding sublattices. The interaction effect is included by considering on-site repulsion between electrons

$$H_U = U \sum_{\mathbf{r} \in \mathbf{R}, i} :n_{i\uparrow}(\mathbf{r})n_{i\downarrow}(\mathbf{r}):, \quad (2.2)$$

where $n_{i\alpha} \equiv c_{i\alpha}^\dagger c_{i\alpha}$ denotes electron density on sublattice i with spin α . Throughout this paper, only repulsive interaction ($U > 0$) is considered.

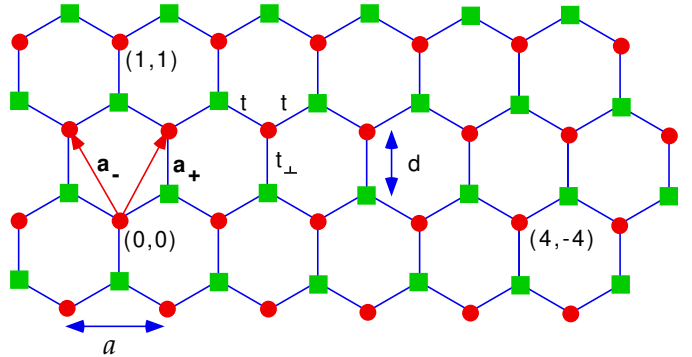


FIG. 1: two dimensional Honeycomb lattice with bases \mathbf{a}_\pm . Circles and squares represent fermion sites on two sublattices separated by a distance $d = a/\sqrt{3}$. A $(1,1)$ -armchair is obtained by rolling up the sheet from $(0,0)$ to $(1,1)$ and end points. Similarly, a $(4,-4)$ -zigzag is obtained by rolling from $(0,0)$ to $(4,-4)$.

In the weak coupling regime $U \ll t, t_\perp$, it is natural to diagonalize the hopping Hamiltonian H_0 first and study the band structure. By going into momentum space, the energy spectrum is $E(\mathbf{k}) = \mp|h(\mathbf{k})|$

$$h(\mathbf{k}) = 2t \cos(k_x a/2)e^{ik_y a/2\sqrt{3}} + t_\perp e^{-ik_y a/\sqrt{3}}, \quad (2.3)$$

where \mathbf{k} is the crystal momentum. The \mp signs in the energy spectrum denote bonding and antibonding bands. Since the undoped graphite sheet is half-filled, the bonding band is completely filled while the antibonding band is empty. One prominent feature of the band structure is that the bonding and antibonding bands are separated by a finite gap everywhere in the Brillouin zone (BZ) except at two peculiar points \mathbf{K}_\pm . They are conventionally called Dirac points because the (gapless) dispersion looks relativistic near them, i.e.

$$E(\mathbf{k}) = v|\mathbf{k} - \mathbf{K}_\pm|. \quad (2.4)$$

For $t_\perp = t$, the Dirac points are located at $\mathbf{K}_\pm = (\pm 4\pi/3a, 0)$ and the Fermi velocity $v = (\sqrt{3}/2)ta$ as shown in Fig. 2. If t_\perp is slightly different from t , these points get shifted a bit along the k_x direction. Equivalent points in the BZ are related by reciprocal lattice vectors. At half-filling (or under slight doping), gapless excitations only exist at (or near) the Dirac points and the low-energy physics is captured by two flavors of Dirac fermions with the on-site interaction in Eq. 2.2. It is strikingly similar to the 2-chain Hubbard model which describes two interacting Dirac fermions with on-site repulsions. This motivates us to search for equivalent 2-chain models for nanotubes near half filling. In the following subsections, we manipulate the (N_y, N_y) -armchair and the $(N_x, -N_x)$ -zigzag with $N_x = 3n$ to show that it is indeed possible to map them into equivalent 2-chain models.

A. Armchair tubes

The (N_y, N_y) -armchair has a finite circumference $C = \sqrt{3}aN_y$ which leads to the quantization of transverse momentum k_y around the tube. In addition to the quantized momenta, the curvature effect causes the slight difference between t, t_{\perp} which shifts the locations of the Dirac points as shown in Fig. 2. Since the quantized momentum ($k_y = 0$) cuts through the Dirac points, the armchair without interactions is expected to be a metal. But once the interaction effect is taken into consideration, the low-energy excitations change dramatically. An armchair carbon nanotube with on-site interaction has been shown equivalent to the 2-chain Hubbard model at or near half filling where only $k_y = 0$ band is gapless. [12] Here we rederive the same mapping by a more systematic method which can also be applied to zigzag tubes later.

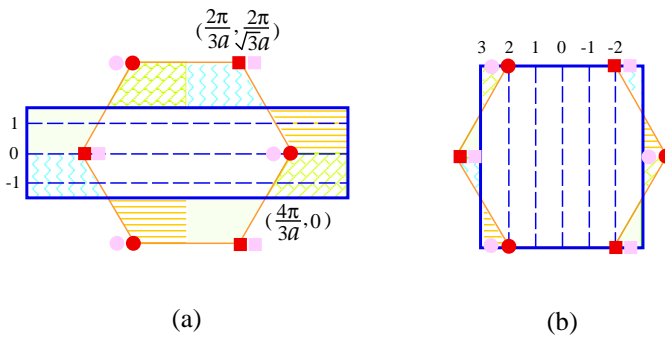


FIG. 2: Dirac points in the Brillouin zone. Dark circles and squares indicate the locations of the Dirac points for $t_{\perp} = t$, and grey symbols for $t_{\perp} < t$. Dashed lines show the allowed quantized momenta in (a) the (3,3)-armchair and (b) the (6,-6)-zigzag. The conventional hexagonal zone is mapped into rectangle one for (a) the armchair and (b) the zigzag.

To proceed with the mapping, the conventional hexagonal BZ needs to be rearranged into a rectangle. With several parts shifted by reciprocal lattice vectors, it is done as shown in Fig. 2(a). It is crucial to make such a change and the reason will become clear later. With the choice of this particular BZ, referred to as BZ(arm) later, the allowed transverse momentum takes N_y integer values

$$k_y = \frac{2\pi}{\sqrt{3}a} \frac{p}{N_y}, \quad p = 0, \pm 1, \pm 2, \dots, (\pm) \left[\frac{N_y}{2} \right], \quad (2.5)$$

where (\pm) means, if N_y is an even number, only one sign is chosen in order to count the total number of modes properly. For notational convenience, we later represent the transverse momentum k_y by the dimensionless integer p . Similarly, since the transverse coordinate y runs through N_y values for each fixed x , it is possible to label it by a dimensionless integer n . The fermion operator $c_i(x, n) \equiv c_i(x, y)$ is then labeled by the integer n defined as

$$n = \begin{cases} \frac{1}{\sqrt{3}a}(y + \delta_{i2}d) & \text{if } x = ma, \\ \frac{1}{\sqrt{3}a}(y + \delta_{i2}d) - \frac{1}{2} & \text{if } x = (m + \frac{1}{2})a, \end{cases} \quad (2.6)$$

where m, n are integers and $n = 1, 2, \dots, N_y$. Since only the $k_y = 0$ mode is important for the armchair at or near half filling, we want to construct fermion operators carrying definite transverse momentum and then discard the non-zero momentum components. The required operator is constructed by partial Fourier transformation in the y -direction

$$\begin{aligned} c_i(x, y) &= \frac{1}{\sqrt{N_y}} \sum_{k_x, k_y} e^{i\mathbf{k} \cdot \mathbf{r}} c_i(k_x, k_y) \\ &\equiv \frac{1}{\sqrt{N_y}} \sum_p e^{i\frac{2\pi}{N_y} np} d_i(x, p), \end{aligned} \quad (2.7)$$

where the normalization constant $N_1 = N_2 = 2N_yL/a$ is the total number of fermion sites on each sublattice and L is the length of the tube. To obtain the second line in Eq. 2.7, we sum over all possible k_x and replace y and k_y by integers n and p respectively. This transformation can be written down in a more compact form

$$c_i(x, n) = S_{np}^{(y)} d_i(x, p), \quad (2.8)$$

$$d_i(x, p) = S_{pn}^{(y)\dagger} c_i(x, n), \quad (2.9)$$

where summation on doubly appeared indices is implied. The transformation matrix $S^{(y)}$ is

$$S_{ab}^{(y)} \equiv \frac{1}{\sqrt{N_y}} \exp(i \frac{2\pi}{N_y} ab). \quad (2.10)$$

This transformation is only possible in the first place because the summation over all momenta in the BZ, \sum_{k_x, k_y} , can be separated into two independent sums, $\sum_{k_y} \sum_{k_x}$, which is a direct result of the rectangular shape. Secondly, with the specific choice of the BZ(arm), the momentum k_y runs through N_y values (given in Eq. 2.5) as the transverse coordinate y . As a result, the transformation matrix $S^{(y)}$ is unitary which preserves the fermionic commutation relations between $d_i(x, p)$

$$\{d_i(x, p), d_j(x', p')\} = \delta_{ij} \delta_{pp'} \delta_{xx'}. \quad (2.11)$$

Since the Dirac points lie on the $k_y = 0$ line, all modes with non-zero transverse momentum are gapped and can be integrated out in the weak coupling. Keeping the zero momentum mode, Eq. 2.8 becomes

$$c_i(x, n) \simeq \frac{1}{\sqrt{N_y}} d_i(x, 0) \equiv \frac{1}{\sqrt{N_y}} d_i(x), \quad (2.12)$$

where the dependence of the coordinate y completely drops out. Within this approximation, the Hamiltonian in Eq. 2.1, 2.2 is mapped to a 2-chain system

$$H_0 = \sum_{x,\alpha} \left\{ -td_{1\alpha}^\dagger(x)d_{2\alpha}(x-b) -td_{1\alpha}^\dagger(x)d_{2\alpha}(x+b) -t_\perp d_{1\alpha}^\dagger(x)d_{2\alpha}(x) + \text{h.c.} \right\}, \quad (2.13)$$

$$H_U = \left(\frac{U}{N_y}\right) \sum_{x,i} : d_{i\uparrow}^\dagger(x)d_{i\uparrow}(x)d_{i\downarrow}^\dagger(x)d_{i\downarrow}(x) :, \quad (2.14)$$

where $b = a/2$ is the lattice constant. The hopping term may not look familiar at first sight. By depicting hoppings between two sublattices explicitly in Fig. 3(a), it is clear that it describes the 2-chain Hubbard model with lattice constant $b = a/2$. It is interesting that the interaction strength reduces to U/N_y . The $1/N_y$ factor can be thought as coming from delocalized electrons around the tube since they would then have a probability $1/N_y$ to occupy the same site. We emphasize that this effective model is only correct when the armchair is at or near half filling, such that the other bands with non-zero transverse momentum are still gapped. Upon larger doping, the interaction effect is more complicated and will be studied in the next section.

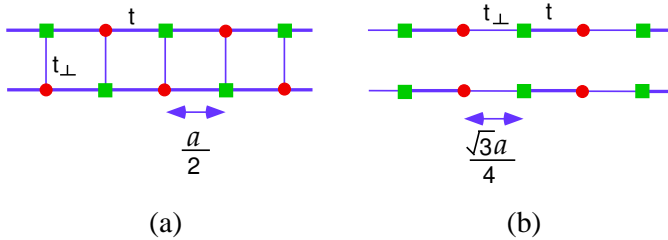


FIG. 3: Effective 2-chain model for (a) the armchair and (b) the zigzag. Squares and circles indicate fermion sites on two sublattices.

The 2-chain Hubbard model has been studied with RG techniques by many authors. Here we adapt the approach and notations in Ref. [15] and briefly review the strategy. First of all, the fermions $d_i(x)$ are relabeled by chain indices in stead of the sublattice indices in Eqs. 2.13, 2.14. Since the coordinate $x = mb$ is an integer multiple of b , in the continuous limit, the sum is replaced by an integral and the fermion fields acquire a rescaling factor

$$b \sum_x \rightarrow \int dx \quad (2.15)$$

$$\frac{1}{\sqrt{b}} d_i(x) = \psi(x, y), \quad (2.16)$$

where $y = 1, 2$ labels different chains. We diagonalize the hopping Hamiltonian in the continuous version and obtain bonding and anti-bonding bands which are denoted by $\psi_i(x)$ with $i \equiv k_y/\pi = 0, 1$. Filling up the bands to the chemical potential energy and linearizing the dispersion around the Fermi points, the fermion fields in bonding

and antibonding bands are approximated by two pairs of chiral fields as

$$\psi_{i\alpha}(x) \sim \psi_{Ri\alpha}(x)e^{ik_{Fi}x} + \psi_{Li\alpha}(x)e^{-ik_{Fi}x}, \quad (2.17)$$

where k_{Fi} is the Fermi momentum of each band. The effective theory contains two flavors of Dirac fermions described by the Hamiltonian

$$\mathcal{H}_0 = \sum_{i\alpha} v_i \{ \psi_{Ri\alpha}^\dagger(x) (-i\partial_x) \psi_{Ri\alpha} + \psi_{Li\alpha}^\dagger(x) i\partial_x \psi_{Li\alpha} \}, \quad (2.18)$$

where v_i is the Fermi velocity of each band. There are many possible interactions between these Dirac fermions but only some of them are relevant to the change of low-energy excitations. For example, an interaction with right (left) moving fields alone only renormalizes the Fermi velocities and can be ignored in the leading order of U . On the other hand, interactions which couple right and left moving fields together can possibly open up a gap. To write down these interactions explicitly, the SU(2) scalar and vector currents are introduced

$$J_{ij} = \psi_i^{\alpha\dagger} \psi_{j\alpha}, \quad \mathbf{J}_{ij} = \frac{1}{2} \psi_i^{\alpha\dagger} \boldsymbol{\sigma}_\alpha^\beta \psi_{j\beta}; \quad (2.19)$$

$$I_{ij} = \psi_{i\alpha} \epsilon^{\alpha\beta} \psi_{j\beta}, \quad \mathbf{I}_{ij} = \frac{1}{2} \psi_{i\alpha} \epsilon^{\alpha\beta} \boldsymbol{\sigma}_\beta^\gamma \psi_{j\gamma}, \quad (2.20)$$

where $\boldsymbol{\sigma}$ is Pauli matrices and $\epsilon^{\alpha\beta}$ is the Levi-Civita antisymmetric tensor with the convention $\epsilon^{12} = -\epsilon^{21} = 1$. All possible interactions which are relevant to gap openings are represented succinctly by these currents

$$\mathcal{H}_{\text{int}} = c_{ij}^\rho J_{ij}^R J_{ij}^L - c_{ij}^\sigma \mathbf{J}_{ij}^R \cdot \mathbf{J}_{ij}^L, + f_{ij}^\rho J_{ii}^R J_{jj}^L - f_{ij}^\sigma \mathbf{J}_{ii}^R \cdot \mathbf{J}_{jj}^L, \quad (2.21)$$

$$\mathcal{H}_{\text{int}}^{(u)} = v_{ij}^{1\rho} I_{ij}^R I_{\hat{i}\hat{j}}^{L\dagger} - v_{ij}^{1\sigma} \mathbf{I}_{ij}^R \cdot \mathbf{I}_{\hat{i}\hat{j}}^{L\dagger} + \text{h.c.}, \quad (2.22)$$

where f_{ij} and c_{ij} denote the forward and Cooper scattering amplitudes respectively, between bands i and j . Umklapp interactions v_{ij}^1 [16] only appear at half filling. Summation on i, j is implied. Because of various symmetries, these couplings are symmetrical. Since $\mathbf{I}_{ii} \equiv 0$ due to the anti-symmetric nature of \mathbf{I}_{ij} , its corresponding coupling $v_{ii}^{1\sigma}$ is always set to zero. Expressing the on-site interaction in Eq. 2.14 in terms of these Dirac fermions, we can compare the results with Eqs. 2.21, 2.22. The initial couplings generated by the on-site interaction are

$$c_{ij}^\sigma = f_{ij}^\sigma = 4c_{ij}^\rho = 4f_{ij}^\rho = \frac{Ub}{N_y}, \quad (2.23)$$

$$v_{01}^{1\rho} = 2v_{ii}^{1\rho} = \frac{Ub}{4N_y}, \quad v_{01}^{1\sigma} = 0, \quad (2.24)$$

where $i, j = 0, 1$ are the band indices. The lattice constant b appears in the continuous limit because these couplings are dimensionless.

With the knowledge of Fermi velocities and initial couplings, we employ the RG equations derived in Ref. [14,15] to determine which couplings are (marginally) relevant and grow into the strong coupling regime when short-ranged fluctuations are integrated out. The phase diagram is then determined by these relevant couplings through the bosonization technique. Numerical results show that, at half filling, the relevant couplings gap out all spin and charge excitations and lead the system to a C0S0 Mott's insulator, where CnSm means there are n gapless charge and m gapless spin modes. The spin and charge gaps change the simple band calculation predictions of the transport properties at low temperature. For instance, the resistivity blows up exponentially when the temperature is cooled down below the gap scale. Upon doping away from half filling, the umklapp interactions are no longer allowed. The Cooper scatterings induce a net attractive interaction between electron at low-energy scale and lead to electron pairings. According to the numerics, the system goes into the C1S0 phase with a gap function of d-wave symmetry. The spin gap comes from the singlet pairing and the only gapless charge mode is the usual U(1) phase in a superconductor.

As one might notice that the results of the RG analysis only depends on two factors: the Fermi velocities calculated from the band structure and the initial couplings generated by the on-site interaction. An alternative interpretation of the effective model for the armchair is available. The Fermi velocities can be calculated directly from the band structure of the armchair without mapping to any effective models. As to the couplings in Eqs. 2.23, 2.24, they are similar to the N -chain Hubbard model with lattice constant b , (e.g. $c_{ij}^\sigma = 2Ub/N$). By comparison, the initial couplings for the (N_y, N_y) -armchair in the $N_f = 2$ region are *identical* to those of the $2N_y$ -chain Hubbard model with two partially filled bands, where N_f is the number of Dirac fermions in the nanotubes. It just happens that the band structure for $k_y = 0$ in the armchair has the same dispersion as in a real 2-chain system, which enables us to find the mapping described before. This new interpretation has the advantage that the equivalence of the couplings holds at generic fillings, where an effective 2-chain model is impossible. The connection between the (N_y, N_y) -armchair and the $2N_y$ -chain Hubbard model is elucidated in detail in the next section.

B. Zigzag tubes

For an $(N_x, -N_x)$ -zigzag tube, the circumference is $C = N_x a$ and the momentum k_x is quantized. The band structure shows interesting results even when interactions are negligible. For now, we ignore the curvature effect and set $t_\perp = t$. For $N_x = 3n$, the Dirac points lie on the allowed momenta (see Fig. 2(b)). The system has gapless excitations and thus is a metal. For

$N_x \neq 3n$, the allowed momenta do not cut through the Dirac points and the (filled) bonding and (empty) anti-bonding bands are separated by a finite gap. Thus, the system is a semi-conductor. Due to curvature effects, the difference between transverse and longitudinal hoppings is of order $1/N_x^2$ [10,11], and it causes a gap Δ also of order $1/N_x^2$ even when $N_x = 3n$. However, we find later that the effective interaction is of order $1/N_x$. It is then reasonable to ignore the minor gap caused by curvature and treat $(3n, -3n)$ -zigzag tubes as metallic. Since $N_x \neq 3n$ tubes are already insulating without interactions, the inclusion of interaction effect does not change the low-energy physics dramatically. We focus on the more interesting case of $N_x = 3n$ and explore whether the interactions can indeed cause gaps.

For the $(3n, -3n)$ -zigzag, a mapping to a 2-chain model, similar to the armchair, is found by partial Fourier transform in x . To perform the transformation, as for the armchair, a rectangular BZ is again necessary. However, the BZ(arm) is not suitable because it contains $2N_x$ quantized k_x which is twice the number of modes necessary to make the transformation unitary. Another BZ is chosen as shown in Fig. 2(b), which is referred to as BZ(zz) later. With this choice, the momentum k_x has N_x allowed values:

$$k_x = \frac{2\pi}{a} \frac{p}{N}, \quad p = 0, \pm 1, \pm 2, \dots, (\pm) \left[\frac{N_x}{2} \right]. \quad (2.25)$$

For each fixed coordinate y , the transverse coordinate x runs through N_x possible values. The fermion field, $c(n, y) \equiv c(x, y)$, is labeled by the integer n defined as

$$n = \begin{cases} x/a & \text{if } y = m\sqrt{3}a, \\ x/a - \frac{1}{2} & \text{if } y = (m + \frac{1}{2})\sqrt{3}a, \end{cases} \quad (2.26)$$

where m, n are integers and $n = 1, 2, \dots, N_x$. The fermion field $d_i(p, y)$ which carries definite momentum k_x is constructed by partial Fourier transformation in x

$$c_i(n, y) = S_{np}^{(x)} d_i(p, y), \quad (2.27)$$

$$d_i(p, y) = S_{pn}^{(x)\dagger} c_i(n, y). \quad (2.28)$$

The transformation matrix $S^{(x)}$ is

$$S_{ab}^{(x)} \equiv \frac{1}{\sqrt{N_x}} \exp\left(i \frac{2\pi}{N_x} ab\right). \quad (2.29)$$

Since $S_{ab}^{(x)}$ is unitary, the fermion field $d_i(p, y)$ obeys the canonical anti-commutators. For $t_\perp = t$, the Dirac points lie on two specific momenta, $k_x = \pm 2\pi/3a$, and other bands acquire major gaps. Even with the inclusion of curvature effects, the gaps of the $k_x = \pm 2\pi/3a$ bands is only of order $1/N_x^2$, which is smaller than those of the other bands. In the weak coupling, it is legitimate to integrate out all other gapped modes and $c_i(x, y)$ only contains components near the Dirac points

$$c_i(x, y) \sim \frac{1}{\sqrt{N_x}} \sum_{q=\pm} d_{qi}(y) e^{iq \frac{2\pi}{3a} x}, \quad (2.30)$$

where $d_{\pm i}(y) \equiv d_i(\pm N_x/3, y)$. Within this approximation, the hopping Hamiltonian in Eq. 2.1 is simplified to two chains without interchain hoppings

$$H_0 = \sum_{y,q=\pm} \left\{ -td_{q1}^\dagger(y)d_{q2}(y+b'+\delta) - t_\perp d_{q1}^\dagger(y)d_{q2}(y-b'+\delta) + \text{h.c.} \right\}, \quad (2.31)$$

where $q = \pm$ is the chain indices. The lattice constant is $b' = \sqrt{3}a/4$ and the distortion distance is $\delta = \sqrt{3}a/12$. The distortion δ can be gauged away by shifting one of the sublattices. Performing a gauge transformation to shift the second sublattice by δ , we get

$$D^\dagger d_{q1}(y)D = d_{q1}(y), \quad (2.32)$$

$$D^\dagger d_{q2}(y+\delta)D = d_{q2}(y). \quad (2.33)$$

In momentum space, this gauge transformation only adds a phase to $d_{q2}(k) \rightarrow d_{q2}(k)e^{ik\delta}$ and does not change the band structure at all. As to the interaction, since it is on-site, it is also invariant under this gauge transformation. The hopping Hamiltonian becomes

$$H_0 = \sum_{y,q} \{-t(y)d_q^\dagger(y)d_q(y+b') + \text{h.c.}\}, \quad (2.34)$$

with the hopping $t(y)$ alternating along the y -direction as

$$t(y) = \frac{1}{2} \{ (t + t_\perp) + (-1)^y (t - t_\perp) \}. \quad (2.35)$$

For $t_\perp \neq t$, the hopping Hamiltonian represents a dimerized chain as shown in Fig. 3(a) and has a gap $\Delta \sim (t_\perp - t)$ while, for $t_\perp = t$, the gap vanishes. This is in agreement with our previous conclusion for the zigzag. As argued before, the minor difference of order $1/N_x^2$ between t , and t_\perp caused by curvature effects is negligible because the interactions are order of $1/N_x$. Thus we set $t = t_\perp$ in the following. It takes a little algebra to write down the interactions between these two chains and obtain

$$H_U = \left(\frac{U}{N_x} \right) \sum_{y,q} \left\{ n_{q\uparrow}(y)n_{q\downarrow}(y) + n_{q\uparrow}(y)n_{\bar{q}\downarrow}(y) + d_{q\uparrow}^\dagger(y)d_{\bar{q}\uparrow}(y)d_{\bar{q}\downarrow}^\dagger(y)d_{q\downarrow}(y) \right\}, \quad (2.36)$$

where the notation $\bar{a} = -a$ is adapted through out the paper. It is interesting to compare the effective 2-chain models for the armchair and the zigzag. For the armchair, the on-site interaction remains simple but there exist hoppings between two chains, while, for the zigzag, there is no hoppings between chains but the interactions are complicated. The effective model obtained here does not look like the 2-chain Hubbard model yet. Following the method for the armchair, we take the continuous

limit and linearize the spectrum near the Fermi points. The fermion fields in these two chains are approximated by two pairs of chiral fermions as

$$\psi_q(y) \sim \psi_{Rq}(y)e^{ik_F q y} + \psi_{L\bar{q}}(y)e^{-ik_F q y}. \quad (2.37)$$

Once more we have an interacting theory with two flavors of Dirac fermions. Because of the absence of interchain hoppings, these two bands are degenerate and, thus, always have the same Fermi velocities. The allowed interactions are the same as those of the armchairs in Eqs. 2.21, 2.22. The initial couplings determined from the interactions in Eq. 2.36 are

$$c_{ij}^\sigma = f_{ij}^\sigma = 4c_{ij}^\rho = 4f_{ij}^\rho = \frac{2Ub'}{N_x}, \quad (2.38)$$

$$v_{01}^{1\rho} = 2v_{ii}^{1\rho} = \frac{Ub'}{2N_x}, \quad v_{01}^{1\sigma} = 0. \quad (2.39)$$

The couplings are exactly the same as for the 2-chain Hubbard model with reduced interaction $u_{\text{eff}} = U/N_x$ and lattice constant $b' = \sqrt{3}a/4$. At half filling, the Fermi velocities of Dirac fermions for the armchair and the $(3n, -3n)$ -zigzag are identically the same. As a result, the effective theory of the zigzag is again described by the 2-chain Hubbard model with reduced interaction U/N_x and lattice constant $b' = \sqrt{3}a/4$. Upon doping, the Fermi velocities of the zigzag remain degenerate and start to deviate from the Hubbard model. However, numerical results show that the phase is still C1S0 as in a doped armchair tube. It is interesting to compare a $(3N, 3N)$ -armchair and $(6N, -6N)$ -zigzag because the effective interaction strength $u_{\text{eff}} = U/3N$ is the same for both. However, since the lattice constant of the armchair b is slightly larger, the initial couplings of the armchair is a bit larger than those of the zigzag. By integrating the RG flow numerically, the results imply that the critical temperature of the armchair is higher than the zigzag due to the difference in the initial couplings from difference lattice constants.

III. NANOTUBES AT GENERIC FILLINGS

So far, we studied the carbon nanotube at fillings described by two flavors of interacting Dirac fermions and found it is closely related to the 2-chain Hubbard model. Upon larger doping, the chemical potential cuts through more pairs of Fermi points and, in general, there are N_f flavors (more than two) of Dirac fermions participating in the interactions. For example, the $(3, 3)$ -armchair enters $N_f = 6$ region upon larger doping as indicated in Fig. 4, while the $(6, -6)$ -zigzag enters $N_f = 4$ region as shown in Fig. 5. The strategy used to analyze them with RG techniques involves two steps: calculate the Fermi velocities from the band structure, and figure out all possible interactions with the initial couplings generated by the on-site interaction. The first step is easy because the band structure of nanotubes is already obtained in Eq. 2.3. The

second step is more challenging. We are going to show that the interactions between these N_f flavors of Dirac fermions are almost the same as in the N -chain Hubbard model in the N_f partially filled band regime. In the following, we focus on the (3,3)-armchair in the $N_f = 6$ region and the (6, -6)-zigzag in the $N_f = 4$ region as examples. The generality of this equivalence is transparent from these two typical illustrations.

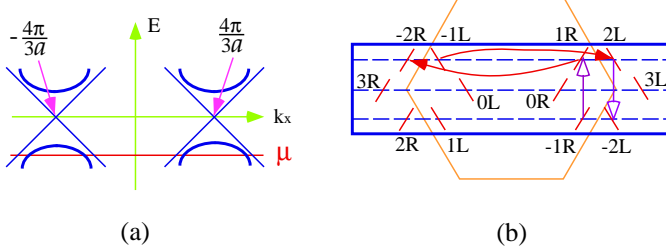


FIG. 4: The (3,3)-armchair in $N_f = 6$ partially filled band region. The band structure near $E = 0$ is shown in (a) and the corresponding Fermi points are also plotted in the BZ in (b). The thick line represents the two degenerate bands with transverse momentum $p = \pm 1$. For each quantized momentum p , there are two flavors of Dirac fermions participating in the interactions. The solid (empty) arrow lines indicate the umklapp coupling u_{12}^1 (u_{12}^2) in addition to the Cooper and forward couplings.

We study the armchair first. For convenience, the sublattice index $i = 1, 2$ in $c_i(x, y)$ is viewed as the z -coordinate. The corresponding momentum $p' \equiv k_z/\pi = 0, 1$ labels the bonding and anti-bonding bands respectively. Perform a partial Fourier transformation in BZ(arm) for both y, z to diagonalize the hoppings around the tube, we get

$$c_i(x, n) = S_{np}^{(y)} S_{ip}^{(z)} c_{\mathbf{p}}(x), \quad (3.1)$$

where $\mathbf{p} = (p, p')$ is the momentum in the y, z directions. The transfer matrix $S^{(z)}$ is defined analogous to $S^{(y)}$ defined in Eq. 2.10

$$S_{ab}^{(z)} = \frac{1}{\sqrt{N_z}} \exp\left(i \frac{2\pi}{N_z} ab\right), \quad (3.2)$$

where the normalization constant $N_z = 2$ accounts for two possible values of $z(k_z)$. In the continuous limit, the fermion field is rescaled as

$$c_{\mathbf{p}}(x) = \sqrt{b} \psi_{\mathbf{p}}(x). \quad (3.3)$$

We linearize the dispersions near each Fermi point and describe the system by $N_f = 6$ flavors of Dirac fermions. Since the system is doped, only the bonding band ($p' = 0$) participates in the interactions. Since the anti-bonding band ($p' = 1$) never appears in the following analysis, the p' index is dropped for notational simplicity. To make the equivalence to the Hubbard model transparent, the fermions are labeled in a particular way:

$$\begin{aligned} \psi_p(x) &\sim \psi_{Rp}(x) e^{ik_{Fp}x} + \psi_{L\bar{p}}(x) e^{-ik_{Fp}x} \\ &+ \psi_{Rp^*}(x) e^{ik_{Fp^*}x} + \psi_{L\bar{p}p^*}(x) e^{-ik_{Fp^*}x}, \end{aligned} \quad (3.4)$$

where $p^* = p - \text{sgn}(p)N_y$. The labeling of these fermions is given explicitly in the Fig. 4. It is straightforward to check that the Cooper and forward scatterings are allowed between any two of the fermions. However, since there are two flavors of Dirac fermions for each k_y , additional interactions are also allowed. Two examples are shown in Fig 4(b). These are the umklapp interactions in the k_y direction

$$\begin{aligned} \mathcal{H}_{\text{int}}^{(uy)} &= u_{ij}^{1\rho} J_{ij}^R J_{ij}^L - u_{ij}^{1\sigma} \mathbf{J}_{ij}^R \cdot \mathbf{J}_{ij}^L, \\ &+ u_{ij}^{2\rho} J_{ii}^R J_{jj}^L - u_{ij}^{2\sigma} \mathbf{J}_{ii}^R \cdot \mathbf{J}_{jj}^L. \end{aligned} \quad (3.5)$$

The name comes from the fact that if the BZ(arm) is shifted back to the the conventional one, the transfer transverse momentum associated with each vertex equals the reciprocal lattice vector $4\pi/\sqrt{3}a$. The allowed interactions are therefore described by Eqs. 2.21, 3.5 as in a doped (even-chain) Hubbard model with periodic boundary conditions. We need to compute the initial couplings generated by the on-site interaction to complete the equivalence. The on-site interaction is expressed in terms of the Dirac feermions as

$$\begin{aligned} H_U &= U \sum_{x,y,z} n_{\uparrow}(x, y, z) n_{\downarrow}(x, y, z) \\ &= U b \int dx \sum_{P_{i_a}, i_a} \left\{ f_{i_1 i_2 i_3 i_4}^{(y)} f_{j_1 j_2 j_3 j_4}^{(z)} \right. \\ &\quad \left. \psi_{P_{i_1} i_1 \uparrow}^{\dagger} \psi_{P_{i_2} i_2 \uparrow}^{\dagger} \psi_{P_{i_3} i_3 \downarrow}^{\dagger} \psi_{P_{i_4} i_4 \downarrow}^{\dagger} e^{iQ_x x} \right\}, \end{aligned} \quad (3.6)$$

where i_a is the momentum index of k_y and run through $N_f = 6$ values. The j_a labels the k_z momentum and is always zero because only the boning band is interactiing. The chirality of the fermions are denoted by $P_{i_a} = R, L$. The phase associated with each vertex is the transfer momentum in x -direction given by,

$$Q_x \equiv -P_{i_1} k_{F i_1} + P_{i_2} k_{F i_2} - P_{i_3} k_{F i_3} + P_{i_4} k_{F i_4}. \quad (3.7)$$

Conservation of crystal momentum requires Q_x equal to one of the reciprocal lattice vectors. If the momentum is not conserved, the phase associated with the vertex oscillates and the vertex is irrelevant in the leading order analysis. The summations of the transformation matrices in the y, z directions are

$$f_{i_1 i_2 i_3 i_4}^{(d)} \equiv \sum_l S_{li_1}^{(d)*} S_{li_2}^{(d)} S_{li_3}^{(d)*} S_{li_4}^{(d)} = \frac{1}{N_d} \delta_{Q_d, G_d}, \quad (3.8)$$

where $d = y, z$ and $Q_d = (-i_1 + i_2 - i_3 + i_4)$ is the transfer momentum and $G_d = 2nN_d$ is the reciprocal lattice vector. The δ -function enforces the crystal momentum

conservation requirement. Putting everything together, the interacting Hamiltonian, in the continuous limit, is

$$H_U = \left(\frac{Ub}{2N_y}\right) \int dx \psi_{P_{i_1}i_1\uparrow}^\dagger \psi_{P_{i_2}i_2\uparrow} \psi_{P_{i_3}i_3\downarrow}^\dagger \psi_{P_{i_4}i_4\downarrow}, \quad (3.9)$$

where summation over all possible vertices P_{i_a}, i_a , constrained by momentum conservation, is implied. These allowed vertices which can be cast into current-current interactions in Eqs. 2.21, 3.5, have been discussed before. The key point here is that the prefactor $Ub/2N_y$ obtained above is indeed *exactly* the same as that of the $2N_y$ -chain Hubbard model with lattice constant $b = a/2$ in the N_f filled band region. Therefore the equivalence of interactions between the (N_y, N_y) -armchair and the $2N_y$ -chain Hubbard model becomes clear.

With the knowledge of this equivalence, the (3,3)-armchair is studied by integrating the RG equations numerically. The results show that the superconductivity in $N_f = 2$ region, i.e. the C1S0 phase is destroyed because the two flavors of Dirac fermion at $k_y = 0$ indeed become completely decoupled and contribute two gapless charge and two spin modes. However, since the relevant couplings between the remaining four flavors of fermions are too complicated, the phase of the armchair in the $N_f = 6$ region remains an open question for future study.

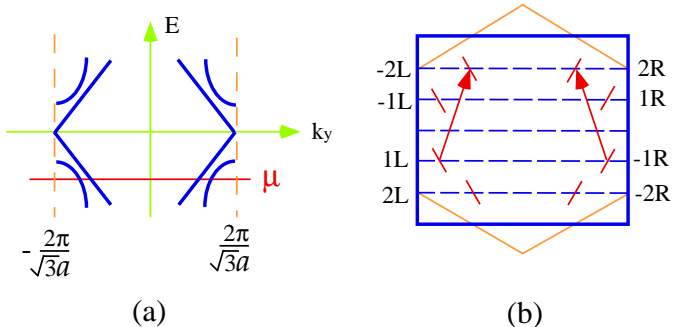


FIG. 5: The (6,-6)-zigzag in $N_f = 4$ partially filled band region. The band structure near $E = 0$ is shown in (a) and the corresponding Fermi points are also plotted in the BZ in (b). The interaction between Band $\pm 1, \pm 2$, as indicated by solid lines, is not allowed because the momentum transfer is *not* a reciprocal lattice vector.

Now we turn to the zigzag. Perform a partial Fourier transformation in both x, z to diagonalize the hoppings around the tube:

$$c(y, m', n') = S_{m'm}^{(x)} S_{n'n}^{(z)} c_{\mathbf{p}}(y), \quad (3.10)$$

Since the coordinate $y = 2nb'$ is an integer multiple of $2b'$, in the continuous limit, the fermion field is rescaled as

$$c_{\mathbf{p}}(y) = \sqrt{2b'} \psi_{\mathbf{p}}(y). \quad (3.11)$$

Linearizing the spectrum near the Fermi points results in following four flavors of Dirac fermions

$$\psi_{\mathbf{p}}(x) \sim \psi_{R\mathbf{p}}(x) e^{ik_{Fp}x} + \psi_{L\bar{\mathbf{p}}}(x) e^{-ik_{Fp}x}. \quad (3.12)$$

The Cooper and forward scatterings are again allowed because the transfer momenta of these vertices are conserved. The k_y umklapp interactions are not allowed because the Fermi momenta do not sum up to the reciprocal lattice vector as shown in Fig. 5. The initial couplings of these interactions are

$$H_U = \left(\frac{Ub'}{N_x}\right) \int dy \psi_{P_{i_1}i_1\uparrow}^\dagger \psi_{P_{i_2}i_2\uparrow} \psi_{P_{i_3}i_3\downarrow}^\dagger \psi_{P_{i_4}i_4\downarrow}. \quad (3.13)$$

This interacting Hamiltonian is the same as the N_x -chain Hubbard model with lattice constant b' in the N_f partially filled band region, except that the k_y umklapp interactions are missing.

With this equivalence, the (6,-6)-zigzag may be studied as follows. Upon doping into the $N_f = 4$ region, the superconductivity vanishes. The bands near the Dirac points are decoupled and contribute 2 gapless charge and 2 spin excitations (C2S2). The remaining two bands form the usual “d-wave” pairing and contribute C1S0. The final phase then is C3S2 and the system no longer has a spin gap. This result shows that the superconductivity only exists inside a narrow window of doping for these nanotubes.

IV. DISCUSSIONS AND CONCLUSIONS

Experimental studies of multi-wall nanotubes show that the electrical properties vary from tube to tube, and are dominated by disorder and weak localization instead of the tubule structure. [17,18] The single-wall nanotubes (SWNT’s) on the other hand have simpler structures and are expected to be more helpful to clear up various interaction effects. Recently, they have been synthesized with high yields and structure uniformity. [6] The (10,10)-armchairs dominate these bulk samples. [19] Tubes during the production process form a 2D triangular lattice (crystalline ropes) and eventually become mats (three dimensional sample with entangled ropes). The (10,10)-armchair is predicted to be metallic (within band calculation) in agreement with experimental evidence. Transport measurements show that the resistivity of the ropes and mats increases linearly with temperature in the high temperature regime and a crossover to negative $d\rho/dT$ happens when temperature goes down. [7] From purely electronic (Coulomb) interactions, it was shown that the umklapp interactions at half filling cause resistivity increases linearly with temperature higher than the Mott’s insulating gap and shoots up exponentially when cooling down below the gap. [12] Another approach also explains the linear resistivity at high temperature by the study of thermal shape fluctuations of these tubes. [11,20] Since the phonons are frozen out at low temperature, the resistivity is expected to go down in contrast to the exponential increase due to umklapp interactions. However the

observed dependence of this crossover on the samples' morphology and quality suggests that disorder or (and) couplings between single tubes may dominate the low temperature behavior. Because the present experimental results are not yet clear in this regime, it will be important to carry out more experiments to understand the origin of this turnover in the resistivity measurements.

Upon doping, both of the (N, N) -armchair and $(3N, -3N)$ -zigzag with on-site interactions become superconductors (SC's) as discussed in the text. Recent studies show that this SC phase is stable with inclusion of moderate nearest neighbor interactions. [21] It implies that the SC phase probably always exists for generic short-range interactions. So far, there is no theoretical work which includes the long-range interaction effect. It would be interesting to see how the unscreened Coulomb repulsion affects this superconducting behavior in the future study.

In conclusion, we represent nanotubes at generic fillings as N_f flavors of interacting Dirac fermions whose velocities are determined by the band structures. With specific on-site type interactions for the (N_y, N_y) -armchair and the $(N_x, -N_x)$ -zigzag, we found the vertices equivalent to those of the $2N_y$ - and N_x -chain Hubbard model respectively, which can be analyzed by the RG method in the weak coupling. With this equivalence, mappings from nanotubes to the effective 2-chain model with reduced couplings are achieved at or near half filling. The $(3,3)$ -armchair and the $(6,6)$ -zigzag are studied and compared as an example because both of them resemble 6-chain systems. At half filling, they are both Mott's insulators and become superconductors upon slight doping. A larger doping to $N_f > 2$ regime destroys the superconductivity.

ACKNOWLEDGMENTS

We are grateful to Matthew P. A. Fisher for motivating the work and many fruitful discussions. We also thank Leon Balents for helpful conversations. This work has been supported by the National Science Foundation

under grant Nos. PHY-9407194, DMR-9400142, DMR-9528578.

- [1] T. Ebbesen, Phys. Today **49**, 26 (1996).
- [2] N. Hamada, S. Sawada, and A. Oshiyama, Phys. Rev. Lett. **68**, 1579 (1992).
- [3] J. Mintmire, B. Dunlap, and C. White, Phys. Rev. Lett. **68**, 631 (1992).
- [4] R. Saito, M. Fujita, G. Dresselhaus, and M. Dresselhaus, Appl. Phys. Lett. **60**, 2204 (1992).
- [5] S. Iijima, Nature **354**, 56 (1991).
- [6] A. Thess *et al.*, Science **273**, 483 (1996).
- [7] J. Fischer *et al.*, Phys. Rev. B **55**, R4921 (1997).
- [8] M. Bockrath *et al.*, Science **275**, 1922 (1997).
- [9] S. Tans *et al.*, Nature **386**, 474 (1997).
- [10] X. Blase, L. Benedict, E. Shirley, and G. Louie, Phys. Rev. Lett. **72**, 1878 (1994).
- [11] C. Kane and E. Mele, Phys. Rev. Lett. **78**, 1932 (1997).
- [12] L. Balents and M. P. A. Fisher, Phys. Rev. B **55**, 11973 (1997).
- [13] Y. Krotov, D.-H. Lee, and G. Louie, cond-mat/9611073 (unpublished).
- [14] L. Balents and M. P. A. Fisher, Phys. Rev. B **53**, 12133 (1996).
- [15] H. H. Lin, L. Balents, and M. P. A. Fisher, cond-mat/9703055 (unpublished).
- [16] The umklapp interactions presented here is in the form which can be generalized to N -chain systems (work in progress by H. H. Lin and A. W. W. Ludwig). The couplings are related to those in Ref. [14] by simple linear combinations.
- [17] H. Dai, E. Wong, and C. Lieber, Science **272**, 523 (1996).
- [18] T. Ebbesen *et al.*, Nature **382**, 54 (1996).
- [19] J. Cowley, P. Nikolaev, A. Thess, and R. Smalley, Chem. Phys. Lett. **265**, 379 (1997).
- [20] C. Kane *et al.*, cond-mat/9704117 (unpublished).
- [21] H. H. Lin, C. L. Kane, M. P. A. Fisher, and L. Balents, preprint (unpublished).